THE FULLY NONCONFORMING VIRTUAL ELEMENT METHOD FOR BIHARMONIC PROBLEMS

P. F. ANTONIETTI, G. MANZINI, AND M. VERANI

ABSTRACT. In this paper we address the numerical approximation of linear fourth-order elliptic problems on polygonal meshes. In particular, we present a novel nonconforming virtual element discretization of arbitrary order of accuracy for biharmonic problems. The approximation space is made of possibly discontinuous functions, thus giving rise to the *fully nonconforming* virtual element method. We derive optimal error estimates in a suitable (broken) energy norm and present numerical results to assess the validity of the theoretical estimates.

1. INTRODUCTION

In recent years the study of numerical methods for the approximation of partial differential equations on polygonal and polyhedral meshes has flourished at exponential rate (see, e.g., the special issues of References [12, 16] for a recent overview of the different methodologies). Among the different proposed methodologies, the Virtual Element Method (VEM), due to its flexibility in dealing with a wide variety of differential problems, has polarized an increasing research activity. VEM has been introduced in the seminal paper [5] and can be seen as an evolution of the Mimetic Finite Difference method, see, e.g., References [13, 33] for a detailed description. Since then, the VEM has been proposed to address an increasing number of different problems: general elliptic problems [9, 17], linear and nonlinear elasticity [6, 29, 14], plate bending [23, 27], Cahn-Hilliard [3], Stokes [2, 15], Helmholtz [36], parabolic [37], Steklov eigenvalue [34], elliptic eigenvalue [30] and discrete fracture networks [18]. Moreover, several different variants of the VEM have been developed and analysed: mixed [21, 8], discontinuous [24], $H(\text{div})$ and $H(\textbf{curl})$-conforming [7], hp [11], serendipity [10] and nonconforming VEM. This latter formulation has been first analyzed

for elliptic problems [4, 26] and subsequently extended to the Stokes problem [25]. Also, very recently, an approximation method for plate bending problems has been analyzed [38], which is based on a globally C^0-nonconforming virtual element space.

In this work we present *the fully nonconforming virtual element method* for the approximation of biharmonic problems. Our method works on unstructured polygonal meshes, provides arbitrary approximation order and does not require any global C^0 regularity for the numerical solution. The numerical approximation of biharmonic problems with nonconforming finite elements on triangular meshes has a very long tradition and it is beyond the scope of this introduction to provide a detailed account of it (see, e.g., the classical book [28] for a short overview). However, it is worth mentioning that as a by product of the results of this paper we obtain, on triangular meshes, a family of novel nonconforming finite elements of *arbitrary* order that are *not* continuous. Indeed, for the lowest order our nonconforming virtual element method on simplicial meshes reduces to the classical Morley element [35], while for higher-order polynomial approximation degrees it gives rise to a new family of nonconforming finite elements.

The outline of the paper is as follows. In Section 2 we recall the continuous problem. In Section 3 we introduce our novel, arbitrary order, nonconforming virtual element discretization for the biharmonic problem. In Section 4 we derive the optimal error estimate in a broken energy norm. In Section 5 we numerically assess the validity of the theoretical estimate and, finally, in Section 6 we draw the conclusions.

1.1. **Notation.** Throughout the paper we shall use the standard notation of the Sobolev spaces $H^m(\mathcal{D})$ for a nonnegative integer m and an open bounded domain $\mathcal{D}$. The m-th seminorm of the function v will be defined by

$$|v|_{m,\mathcal{D}} = \sum_{|\alpha|=m} \left\| \frac{\partial^{|\alpha|} v}{\partial_{x_1}^{\alpha_1} \partial_{x_2}^{\alpha_2}} \right\|_{0,\mathcal{D}}^2,$$

where $\|\cdot\|_{0,\mathcal{D}}^2$ stands for the $L^2(\mathcal{D})$ norm and we set $|\alpha| = \alpha_1 + \alpha_2$ for the nonnegative multi-index $\alpha = (\alpha_1, \alpha_2)$. For any integer $m \geq 0$, $\mathbb{P}^m(\mathcal{D})$ is the classical space of polynomials of total degree up to m defined on $\mathcal{D}$. Moreover, $n = (n_1, n_2)$ is the outward unit normal vector to $\partial\mathcal{D}$, the boundary of $\mathcal{D}$, and $t = (t_1, t_2)$ the unit tangent vector in the counterclockwise orientation of the boundary. To ease the notation, we may use $u_{,i}$ to indicate the first order derivative along the i-th direction, and, accordingly, $u_{,n}$ and $u_{,t}$ for the normal and tangential derivatives. Whenever convenient, we shall also use the notation $\partial_n u$ and $\partial_t u$ instead of $u_{,n}$ and $u_{,t}$. Moreover, we may denote high-order derivatives by repeating the index subscripts, e.g., $u_{,ij} = \partial^2 u / \partial x_i \partial x_j$, and, likewise, $u_{,nn}$, $u_{,tt}$, $u_{,nnt}$, etc, for multiple derivatives in the normal and tangential directions. We also use the summation convention of repeated indexes (Einstein's convention), so that

$$u_{,ij} v_{,ij} = \sum_{ij=1}^{2} \frac{\partial^2 u}{\partial x_i \partial x_j} \frac{\partial^2 v}{\partial x_i \partial x_j}.$$

Finally, the notation $A \lesssim B$ will signify that $A \leq cB$ for some positive constant c independent of the discretization parameters.

2. The continuous problem

Let $\Omega \subset \mathbb{R}^2$ be a convex polygonal domain occupied by the plate with boundary Γ and let $f \in L^2(\Omega)$ be a transversal load acting on the plate. According to the Kirchoff-Love model for thin plates [31] and assuming that the plate is clamped all over the boundary, the transversal displacement u is solution to the following problem

(1a)
$$D\Delta^2 u = f \quad \text{in } \Omega$$

(1b)
$$u = 0 \quad \text{on } \Gamma$$

(1c)
$$\partial_n u = 0 \quad \text{on } \Gamma$$

where $D = \frac{Et^3}{12(1-\nu^2)}$ is the bending rigidity, t being the thickness, E the Young modulus, and ν the Poisson's ratio.

Consider the functional space $V = \left\{ v \in H^2(\Omega) : v = \partial_n v = 0 \text{ on } \Gamma \right\}$ and denote by $\langle \cdot, \cdot \rangle$ the duality pairing between V and its dual V^*.

The variational formulation of (1) reads as: *Find $u \in V$ such that*

(2)
$$a(u, v) = \langle f, v \rangle \qquad \forall v \in V,$$

where

(3)
$$a(u, v) = D \int_\Omega \left(\nu \Delta u \Delta v + (1 - \nu) u_{,ij} v_{,ij} \right) dx \quad \text{and} \quad \langle f, v \rangle = \int_\Omega f v dx.$$

Setting $\| \cdot \|_V = | \cdot |_{2,\Omega}$ and employing the boundary conditions and Poincaré inequality, we can prove that $\| \cdot \|_V$ is a norm on V. Moreover, it holds that

(4a)
$$a(v, v) \gtrsim \|v\|_V^2 \qquad \forall v \in V$$

(4b)
$$|a(u, v)| \lesssim \|u\|_V \|v\|_V \qquad \forall u, v \in V.$$

Hence, there exists a unique solution $u \in V$ to (2) (see, e.g., [19]).

2.1. **Preliminaries.** In this section, we collect some useful definitions that will be employed in the rest of the paper. Let $\sigma_{ij}(u) = \lambda(u_{,11} + u_{,22})\delta_{ij} + \mu u_{,ij}$ with Lamé parameters $\lambda = D\nu$, $\mu = D(1 - \nu)$. We set

(5)
$$M_{nn}(u) = \sigma_{ij}(u)n_i n_j, \quad M_{nt}(u) = \sigma_{ij}(u)n_i t_j, \quad T(u) = \sigma_{ij,j}(u)n_i + M_{nt,t}(u),$$

(we recall the summation notation of repeated indexes) and observe that

$$M_{nn}(u) = \Delta u - (1 - \nu)u_{,tt} = \nu\Delta u + (1 - \nu)u_{,nn},$$

(6)
$$M_{nt}(u) = u_{,nt},$$

$$T(u) = \partial_n(\Delta u) + (1 - \nu)u_{,ntt}.$$

Moreover, let $K \subset \mathbb{R}^2$ be a polygonal domain and set

$$a^K(u,v) = D \int_K \left(\nu \Delta u \Delta v + (1-\nu) \, u_{,ij} v_{,ij} \right) dx.$$

Integrating by parts and employing (5) and (6) yield the following useful identities

$$a^K(u,v) = D \left\{ \int_K \Delta^2 uv dx + \int_{\partial K} \left(\Delta u - (1-\nu)u_{,tt} \right) v_{,n} ds \right.$$

$$\left. - \int_{\partial K} \left(\partial_n(\Delta u)v - (1-\nu)u_{,nt}v_{,t} \right) ds \right\}$$

$$(7) \qquad = D \left\{ \int_K \Delta^2 uv dx + \int_{\partial K} M_{nn}(u)\partial_n v \, ds - \int_{\partial K} T(u)v ds - \sum_{e \in \partial K} \left(M_{nt}(u), vn_{\partial e} \right)_{\partial e} \right\}$$

where ∂e is the boundary of edge $e \subseteq \partial K$ and $n_{\partial e}$ is the outwards normal "vector" to ∂e. For every edge e with end points v_1 and v_2 the boundary ∂e is the set $\{\mathsf{v}_1, \mathsf{v}_2\}$, and, depending on the chosen edge orientation, $n_{\partial e}$ at the end points is equal to $+1$ or -1.

3. Nonconforming virtual element discretization

The nonconforming virtual element approximation of the variational problem (1) reads as: *Find $u_h \in V_{h,\ell}$ such that*

$$(8) \qquad a_h(u_h, v_h) = \langle f_h, v_h \rangle \qquad \forall v_h \in V_{h,\ell},$$

where $V_{h,\ell}$ is the nonconforming virtual element space of order ℓ that approximates the functional space V, and $a_h(\cdot, \cdot)$ and $\langle f_h, \cdot \rangle$ are the nonconforming virtual element bilinear form and load term that approximate $a(\cdot, \cdot)$ and $\langle f, \cdot \rangle$ in (2), respectively. The rest of this section is devoted to the construction of these quantities.

3.1. **Technicalities.** Let $\{\mathcal{T}_h\}_h$ be a sequence of decompositions (meshes) of Ω into non-overlapping polygons K. Each mesh $\mathcal{T}_h$ is labeled by the mesh size parameter h, which will be defined below, and satisfies a few regularity assumptions that are necessary to prove the convergence of the method and derive an estimate of the approximation error. These regularity assumptions are introduced and discussed in Section 4. Let $\mathcal{E}_h$ be the set of edges in $\mathcal{T}_h$ such that $\mathcal{E}_h = \mathcal{E}_h^i \cup \mathcal{E}_h^\Gamma$, where $\mathcal{E}_h^i$ and $\mathcal{E}_h^\Gamma$ are the set of interior and boundary edges, respectively. Similarly, we denote by $\mathcal{V}_h = \mathcal{V}_h^i \cup \mathcal{V}_h^\Gamma$ the set of vertices in $\mathcal{T}_h$, where $\mathcal{V}_h^i$ and $\mathcal{V}_h^\Gamma$ are the sets of interior and boundary vertices, respectively. Accordingly, $\mathcal{V}_h^K$ is the set of vertices of K. Moreover, $|K|$ and $|e|$ denotes the area of cell K and the length of edge e, ∂K is the boundary of K, h_K is the diameter of K and the mesh size parameter is defined as $h = \max_{K \in \mathcal{T}_h} h_K$. We introduce the broken Sobolev space for any integer number $s > 0$

$$H^s(\mathcal{T}_h) = \Pi_{K \in \mathcal{T}_h} H^s(K) = \left\{ v \in L^2(\Omega) : v_{|K} \in H^s(K) \text{ for any } K \in \mathcal{T}_h \right\}$$

and endow it with the broken H^s-seminorm $|v|^2_{s,h} = \sum_{K \in \mathcal{T}_h} |v|^2_{s,K}$.   We denote the traces of v on $e \subset \partial K^+ \cap \partial K^-$ from the interior of $K^\pm$ by $v^\pm$, respectively. Then, we define the jump of v on the interior edge $e \in \mathcal{E}^i_h$ by $[v] = v^+ - v^-$ and on the boundary edge $e \in \mathcal{E}^\Gamma_h$ by $[v] = v_{|e}$.

For future use, we also introduce the nonconforming space $H^{2,nc}(\mathcal{T}_h) \subset H^2(\mathcal{T}_h)$ defined as follows

$$H^{2,nc}(\mathcal{T}_h) = \left\{ v \in H^2(\mathcal{T}_h) : v \text{ continuous at internal vertexes, } v_h(\mathsf{v}_i) = 0 \ \forall \mathsf{v}_i \in \mathcal{V}^\Gamma_h \right.$$

$$\left. \int_e [\partial_n v] ds = 0 \ \forall e \in \mathcal{E}_h \right\}.$$

We next prove the following result.

Lemma 1. $|\cdot|_{2,h}$ *is a norm on both* V *and* $H^{2,nc}(\mathcal{T}_h)$.

Proof. Employing [20, Corollary 4.2] and [20, (5.2)] (with $\Phi(v)$ chosen as in [20, Example 2.6]) we can prove that

$$|v|_{1,h} \lesssim |v|_{2,h} \qquad \forall v \in H^{2,nc}(\mathcal{T}_h)$$

which implies that $|v|_{2,h}$ is a norm on $H^{2,nc}(\mathcal{T}_h)$. $\square$

3.2. **Local and global nonconforming virtual element space.** In this section, we introduce the local and global nonconforming virtual element spaces.

For $\ell \geq 2$, the local virtual element space is defined as follows:

$$V^K_{h,\ell} = \left\{ v_h \in H^2(K) : \Delta^2 v_h \in \mathbb{P}^{\ell-4}(K), M_{nn}(v_h)_{|e} \in \mathbb{P}^{\ell-2}(e), T(v_h) \in \mathbb{P}^{\ell-3}(e) \ \forall e \in \partial K \right\}$$

with the usual convention that $\mathbb{P}^{-1}(K) = \mathbb{P}^{-2}(K) = \{0\}$. The solution of the biharmonic problem in the definition of $V^K_{h,\ell}$ is uniquely determined up to a linear function that can be filtered out by fixing the value at three non-aligned vertexes of K.

Remark 1. *By construction, it holds that* $\mathbb{P}^\ell(K) \subset V^K_{h,\ell}$.

We choose the *degrees of freedom* of $V^K_{h,\ell}$ as follows:

(D1) for $\ell \geq 2$: $v_h(\mathsf{v}_i)$ for any vertex v_i of K;

(D2) for $\ell \geq 2$: $\displaystyle\int_e \partial_n v_h \, p \, ds$ for any $p \in \mathbb{P}^{\ell-2}(e)$ and any edge e of ∂K;

(D3) for $\ell \geq 3$: $\displaystyle\frac{1}{|e|} \int_e v_h p \, ds$ for any $p \in \mathbb{P}^{\ell-3}(e)$ and any edge e of ∂K;

(D4) for $\ell \geq 4$: $\displaystyle\frac{1}{|K|} \int_K v_h p \, ds$ for any $p \in \mathbb{P}^{\ell-4}(K)$.

These degrees of freedom are illustrated in Figure 1 for the virtual element spaces with $\ell = 2, 3, 4, 5$. We next show that these degrees of freedom are unisolvent in $V^K_{h,\ell}$.
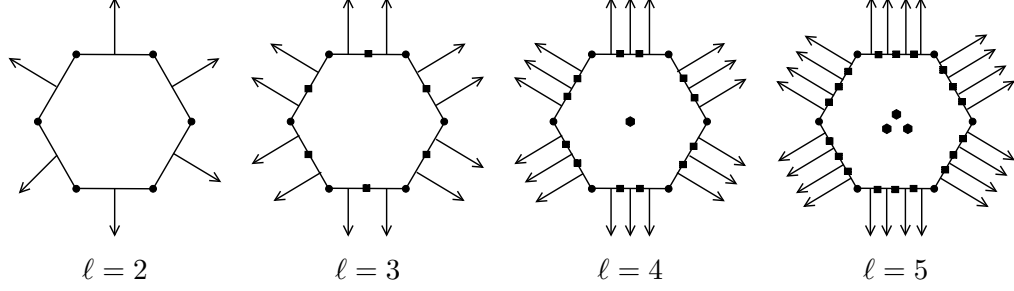
FIGURE 1. Local degrees of freedom of $V_{h,\ell}^K$ for $l = 2, 3, 4, 5$: vertex values $u_h(\mathsf{v})$ (dots); edge moments of $\partial_n u_h$ (arrows); edge moments of u_h (squares); cell moments of u_h (central dots).

Lemma 2. *The degrees of freedom (D1)-(D4) are unisolvent for $V_{h,\ell}^K$.*

Proof. Employing (7), for any $v_h \in V_{h,\ell}^K$ there holds

$$a^K(v_h, v_h) = D\Big\{ \int_K \Delta^2 v_h\, v_h\, dx + \int_{\partial K} M_{nn}(v_h)\partial_n v_h\, ds - \int_{\partial K} T(v_h)\partial_n v_h\, ds$$

$$(9) \qquad\qquad - \sum_{e \in \partial K} (M_{nt}(v_h), v_h n_{\partial e})_{\partial e} \Big\}.$$

We first observe that $\Delta^2 v_h$ is a polynomial of order $\ell - 4$ on K. Moreover, we note that on each edge the functions $M_{nn}(v_h)$ and $T(v_h)$ are polynomial of degree up to $\ell - 2$ and $\ell - 3$, respectively. Hence, by setting to zero the degrees of freedom we get $a^K(v_h, v_h) = 0$. This latter implies $|v_h|_{H^2(K)} = 0$ which gives $v_h = 0$ in view of the fact that setting to zero the nodal values of v_h filters the linear polynomials (i.e. the kernel of the seminorm $|\cdot|_{H^2(K)}$). $\qquad\square$

Building upon the local spaces $V_{h,\ell}^K$, the global nonconforming virtual element space is then defined as follows

$$V_{h,\ell} = \Big\{ v_h : v_h|_K \in V_{h,\ell}^K, v_h \text{ continuous at internal vertexes}, v_h(\mathsf{v}_i) = 0\ \forall \mathsf{v}_i \in \mathcal{V}_h^\Gamma$$

$$(10) \qquad \int_e [\partial_n v_h] p\, ds = 0\ \forall p \in \mathbb{P}^{\ell-2}(e), \int_e [v_h] p\, ds = 0\ \forall p \in \mathbb{P}^{\ell-3}(e)\ \forall e \in \mathcal{E}_h \Big\}.$$

We observe that by construction it holds $V_{h,\ell} \subset H^{2,nc}(\mathcal{T}_h)$ and $V_{h,\ell} \not\subseteq H_0^2(\Omega)$. Moreover, it is important to remark that our nonconforming virtual element space does not require that its functions are globally continuous over Ω, thus admitting piecewise discontinuous functions on each partition $\mathcal{T}_h$ (see also Remark 2 below).

Remark 2 (Lowest order case). *Let us briefly comment on the lowest-order VE space, for $\ell = 2$. In this case the local space is given by*

$$V_{h,2}^K = \left\{ v_h \in H^2(K) : \Delta^2 v_h = 0, M_{nn}(v_h)_{|e} \in \mathbb{P}^0(e), T(v_h)_{|e} = 0 \quad \forall e \in \partial K \right\},$$

and the local degrees of freedom are:

(d1) $v_h(\mathsf{v}_i)$ for any vertex v_i of K;

(d2) $\int_e \partial_n v_h ds$ for any edge e of ∂K.

On triangular meshes the degrees of freedom (d1)-(d2) of V_h^K are the same of the Morley's nonconforming finite element space [35] and the unisolvence property from Lemma 2 implies that these two local spaces coincide. Finally, the global lowest-order nonconforming virtual element space is given by

$$V_{h,2} = \left\{ v_h : v_h|_K \in V_h^K, \ v_h \text{ continuous at internal vertexes, } v_h(\mathsf{v}_i) = 0 \ \forall \mathsf{v}_i \in \mathcal{V}_h^\Gamma, \right.$$

$$\left. \text{and} \int_e [\partial_n v_h] ds = 0 \ \forall e \in \mathcal{E}_h \right\}$$

and clearly contains functions that are piecewise discontinuous on $\mathcal{T}_h$.

3.3. Construction of the bilinear form.

Starting from the local bilinear forms $a_h^K(\cdot, \cdot) : V_{h,\ell}^K \times V_{h,\ell}^K \to \mathbb{R}$ the global bilinear form $a_h(\cdot, \cdot)$ is assembled in the usual way:

$$a_h(u_h, v_h) = \sum_{K \in \mathcal{T}_h} a_h^K(u_h, v_h).$$

Each local bilinear form is given by

$$(11) \qquad a_h^K(u_h, v_h) = a^K\left(\Pi_\ell^{\Delta,K} u_h, \Pi_\ell^{\Delta,K} v_h\right) + S^K\left(\left(I - \Pi_\ell^{\Delta,K}\right)u_h, \left(I - \Pi_\ell^{\Delta,K}\right)v_h\right),$$

where $\Pi_\ell^{\Delta,K}$ is the elliptic projection operator discussed below and $S^K(u_h, v_h)$ is a symmetric and positive definite bilinear form such that

$$a^K(v_h, v_h) \lesssim S^K(v_h, v_h) \lesssim a^K(v_h, v_h)$$

for all $v_h \in V_{h,\ell}^K$ such that $\Pi_\ell^{\Delta,K} v_h = 0$. A practical and very simple choice for $S^K(\cdot, \cdot)$ is the Euclidean scalar product associated to the degrees of freedom scaled by factor h_k^{-2}.

The operator $\Pi_\ell^{\Delta,K} : V_{h,\ell}^K \to \mathbb{P}^\ell(K)$ is the solution of the elliptic projection problem:

$$(12) \qquad\qquad a^K(\Pi_\ell^{\Delta,K} v_h, p) = a^K(v_h, p) \qquad\qquad \forall p \in \mathbb{P}^\ell(K),$$

$$(13) \qquad\qquad ((\Pi_\ell^{\Delta,K} v_h, p))_K = ((v_h, p))_K \qquad\qquad \forall p \in \mathbb{P}^1(K),$$

where

$$((v_h, w_h))_K = \sum_{\mathsf{v} \in \mathcal{V}_h^K} v_h(\mathsf{v}) \, w_h(\mathsf{v}).$$

It is immediate to verify that $\Pi_\ell^{\Delta,K}$ is a projector onto the space of polynomials $\mathbb{P}^\ell(K)$. Indeed, for any $q \in \mathbb{P}^\ell(K)$ equation (12) with $p = \Pi_\ell^{\Delta,K}q - q$ yields $(\Pi_\ell^{\Delta,K}q)_{,ij} = q_{,ij}$ for $i,j = 1,2$. This latter relation combined with (13) proves the assertion. Furthermore, as stated by the following lemma, the polynomial projection $\Pi_\ell^{\Delta,K}v_h$ is computable from the degrees of freedom of v_h.

Lemma 3. *The projector* $\Pi_\ell^{\Delta,K} : V_{h,\ell}^K \to \mathbb{P}^\ell(K)$ *can be computed using only the degrees of freedom (D1)-(D4).*

Proof. In view of (12) and assuming, as usual, the computability of $a^K(p,q)$ for polynomial functions p, q, it is sufficient to prove the computability of $a^K(p,v_h)$ for any $p \in \mathbb{P}^\ell(K)$ and $v_h \in V_{h,\ell}^K$. Employing (7) we have

$$a^K(p,v_h) = D\left\{ \int_K \Delta^2 p v_h dx + \int_{\partial K} M_{nn}(p)\partial_n v_h ds - \int_{\partial K} T(p)v_h ds \right.$$

$$\left. - \sum_{e\in\partial K} \left(M_{nt}(p), v_h n_{\partial e}\right)_{\partial e} \right\}.$$

Each term of the right-hand side can be computed using only the degrees of freedom (D1)-(D4). Indeed, for the first term we note that $\Delta^2 p$ is a polynomial of order $\ell - 4$; for the second term we note that $M_{nn}(p)$ is a polynomial of order $\ell - 2$ on each edge; for the third term we note that $T(p)$ is a polynomial of degree $\ell - 3$; finally, we note that the last term depends on the value of v_h at the vertexes of K. $\qquad\square$

The local bilinear form a_h^K has the two crucial properties of polynomial consistency and stability that we state in the following lemma.

Lemma 4.

- ℓ-**consistency**: *For any* $p \in \mathbb{P}^\ell(K)$ *and any* $v_h \in V_{h,\ell}^K$ *it holds that:*

$$(14) \qquad\qquad a_h^K(p,v_h) = a^K(p,v_h).$$

- **stability**: *For any* $v_h \in V_{h,\ell}^K$ *it holds that:*

$$(15) \qquad\qquad a^K(v_h,v_h) \lesssim a_h^K(v_h,v_h) \lesssim a^K(v_h,v_h),$$

  where the hidden constants are independent of h and K (but may depend on ℓ).

The proof is straightforward, and is therefore omitted.

3.4. **Construction of the load term.** Let Π_K^ℓ denote the L^2-projection onto $\mathbb{P}^\ell(K)$ and f_h be the piecewise polynomial approximation of f on $\mathcal{T}_h$ given by

$$(16) \qquad\qquad f_{h|K} = \Pi_K^{\ell-2} f$$

for $\ell \geq 2$ and every $K \in \mathcal{T}_h$. Then, we set

$$(17) \qquad \langle f_h, v_h \rangle = \sum_{K \in \mathcal{T}_h} \int_K f_h v_h \, dx.$$

In view of (16) and using the definition of the L^2-projection we find that

$$(18) \quad \langle f_h, v_h \rangle = \sum_{K \in \mathcal{T}_h} \int_K \Pi_K^{\ell-2} f v_h \, dx = \sum_{K \in \mathcal{T}_h} \int_K \Pi_K^{\ell-2} f \Pi_K^{\ell-2} v_h \, dx = \sum_{K \in \mathcal{T}_h} \int_K f \Pi_K^{\ell-2} v_h \, dx.$$

The right-hand side of (18) is computable by using the degrees of freedom (D1)-(D4) and the enhanced approach [1] that considers the augmented local space

$$W_{h,\ell}^K = \left\{ v_h \in H^2(K) : \Delta^2 v_h \in \mathbb{P}^{\ell-2}(K), \, M_{nn}(v_h)_{|e} \in \mathbb{P}^{\ell-2}(e), \, T(v_h) \in \mathbb{P}^{\ell-3}(e) \, \forall e \in \partial K, \right.$$

$$\left. \int_K \Pi_\ell^{\Delta,K} v_h p \, dx = \int_K v_h p \, dx \, \forall p \in \mathbb{P}^{\ell-2} \setminus \mathbb{P}^{\ell-4} \right\}.$$

Since (D1)-(D4) are still unisolvent in $W_{h,\ell}^K$, we can compute the projection $\Pi_K^{\ell-2}$ from the degrees of freedom of v_h.

Finally, from (18), employing the Cauchy-Schwarz inequality, standard approximation error estimates and (1) we have the estimate

$$(19) \qquad \langle f - f_h, v_h \rangle = \sum_{K \in \mathcal{T}_h} \int_K \left(I - \Pi_K^{\ell-2}\right) f \left(I - \Pi_K^0\right) v_h \, dx \lesssim h^\ell |v_h|_{2,h},$$

which will be useful in the error analysis of the next section.

4. ERROR ESTIMATES

We now turn to the derivation of an optimal error estimate for the virtual element discretization (8).

On the mesh sequence $\{\mathcal{T}_h\}_h$ we make the following regularity assumptions:

(**H**) there exists a fixed number $\rho_0 > 0$ independent of $\mathcal{T}_h$, such that for every element K it holds:

  (H1) K is star-shaped with respect to all the points of a ball of radius $\rho_0 h_K$

  (H2) every edge $e \in \mathcal{E}_h$ has length $|e| \geq \rho_0 h_K$.

  (H3) There exists a point x_B interior to K such that the sub-triangulation obtained by connecting x_B to the vertices of K is made of shape regular triangles.

The assumptions (H1)-(H2) are standard (see, e.g., [5]) while (H3) is required to perform the error analysis (see, in particular, (23) and (24) in the proof of Theorem 2).

In view of the assumptions (H1)-(H2) on $\mathcal{T}_h$, we can define, for every smooth enough function w, an "interpolant" in $V_{h,\ell}$ with the right interpolation properties. More precisely,

if $\chi_i(w)$, $i = 1,\ldots,\mathcal{N}$, denotes the i-th global degree of freedom of a sufficiently regular function w, there exists a unique element $w^I \in V_{h,\ell}$ such that

$$\chi_i(w - w^I) = 0 \qquad i = 1, 2, \ldots, \mathcal{N}.$$

Moreover, combining Bramble-Hilbert technique and scaling arguments (see e.g. [5, 34] and [19]) as in the finite element framework we can prove that

$$\|w - w^I\|_{s,\Omega} \lesssim Ch^{\beta-s}|w|_{\beta,\Omega} \qquad s = 0, 1, 2 \quad 3 \leq \beta \leq k + 1.$$

In accordance with the seminal paper [32] (see also [28]) we obtain the following result.

Theorem 1. *Under the regularity mesh assumptions (H1)-(H2), there exists a unique solution $u_h \in V_{h,\ell}$ to (8). Moreover, for every approximation $u_\pi \in \mathbb{P}^\ell(\mathcal{T}_h)$ of the exact solution u of (2), it holds that*

$$(20) \qquad |u - u_h|_{2,h} \lesssim (|u - u^I|_{2,h} + |u - u_\pi|_{2,h} + \sup_{v_h \in V_{h,\ell}} \frac{\langle f - f_h, v_h \rangle}{|v_h|_{2,h}} + \sup_{v_h \in V_{h,\ell}} \frac{\mathcal{N}(u, v_h)}{|v_h|_{2,h}},$$

where $u^I \in V_{h,\ell}$ is the interpolant of u in the virtual element space $V_{h,\ell}$ and

$$\mathcal{N}(u, v_h) = \langle f, v_h \rangle - \sum_{K \in \mathcal{T}_h} a^K(u, v_h)$$

$$(21) \qquad = D \sum_{K \in \mathcal{T}_h} \left\{ \int_{\partial K} (\Delta u - (1-\nu)u_{,tt})v_{h,n}ds - \int_{\partial K} \left(\partial_n(\Delta u)v_h - (1-\nu)u_{,nt}v_{h,t}\right) ds \right\}$$

is the non-conformity error.

Proof. Existence and uniqueness of the discrete solution follows easily from the Lax-Milgram theorem by observing that $a_h(\cdot,\cdot)$ is continuous and coercive with respect to $|\cdot|_{2,h}$, which is a norm in $H^{2,nc}$ in view of Lemma 1, and thus on $V_{h,\ell}$ for any $\ell \geq 2$, cf. (10). We now address the proof of (20). Using the triangular inequality we have that

$$|u - u_h|_{2,h} \leq |u - u^I|_{2,h} + |u_h - u^I|_{2,h}.$$

Setting $\delta_h = u_h - u^I$, employing (15) and (7) we obtain the developments

$$
\begin{aligned}
|\delta_h|_{2,h}^2 &= \sum_{K \in \mathcal{T}_h} a^K(\delta_h, \delta_h) \lesssim \sum_{K \in \mathcal{T}_h} a_h^K(\delta_h, \delta_h) \\
&= a_h(u_h, \delta_h) - a_h(u^I, \delta_h) = \langle f_h, \delta_h \rangle - a_h(u^I, \delta_h) \\
&= \langle f_h, \delta_h \rangle - \sum_{K \in \mathcal{T}_h} a_h^K(u^I - u_\pi, \delta_h) - \sum_{K \in \mathcal{T}_h} a_h^K(u_\pi, \delta_h) \\
&= \langle f_h, \delta_h \rangle - \sum_{K \in \mathcal{T}_h} a_h^K(u^I - u_\pi, \delta_h) - \sum_{K \in \mathcal{T}_h} a^K(u_\pi, \delta_h) \\
&= \langle f_h, \delta_h \rangle - \sum_{K \in \mathcal{T}_h} a_h^K(u^I - u_\pi, \delta_h) + \sum_{K \in \mathcal{T}_h} a^K(u - u_\pi, \delta_h) - \sum_{K \in \mathcal{T}_h} a^K(u, \delta_h) \\
&= \langle f_h - f, \delta_h \rangle + \mathcal{N}(u, \delta_h) - \sum_{K \in \mathcal{T}_h} a_h^K(u^I - u_\pi, \delta_h) + \sum_{K \in \mathcal{T}_h} a^K(u - u_\pi, \delta_h),
\end{aligned}
$$

from which inequality (21) follows. $\qquad\square$

Finally, from the above result and bounding each term in (20) we obtain an estimate of the approximation error in the broken energy norm as stated in the following theorem.

Theorem 2. *Let us assume that the solution to (2) satifies $u \in H^3(\Omega)$. Under the regularity assumption* (**H**) *on the mesh $\mathcal{T}_h$, for $\ell \geq 2$ the unique solution $u_h \in V_{h,\ell}$ to (8) satisfies the following error estimate*

$$
\tag{22} |u - u_h|_{2,h} \lesssim h^{\ell-1}.
$$

Proof. In order to prove (22) it is sufficient to combine (19) with (20), use standard interpolation error estimates and the estimate of the conformity error $\mathcal{N}(u, \delta_h)$. Let us focus on the last step. Assuming that u is sufficiently smooth we rewrite the conformity error as follows:

$$
\begin{aligned}
\mathcal{N}(u, \delta_h) = D \sum_{e \in \mathcal{E}_h} &\left\{ \int_e (\Delta u - (1-\nu)u_{,tt})[\delta_{h,n}]ds - \int_e \partial_n(\Delta u)[\delta_h]ds + \int_e (1-\nu)u_{,nt}[\delta_{h,t}]ds \right\} \\
&= D(I + II + III).
\end{aligned}
$$

To estimate the above terms we employ the fact that δ_h belongs to $V_{h,\ell}$ and use standard interpolation error estimates for the L^2-projection Π_e^ℓ on polynomials defined on e. In particular, for the first term for $\ell \geq 2$ we use the definition of the global virtual element space $V_{h,\ell}$ and we find that

$$
\begin{aligned}
I &= \sum_{e \in \mathcal{E}_h} \int_e (I - \Pi_e^{\ell-2})(\Delta u - (1-\nu)u_{,tt})(I - \Pi_e^0)[\delta_{h,n}]ds \\
&\lesssim h^{\ell-2+1-\frac{1}{2}} h^{\frac{1}{2}} |\delta_h|_{2,h} = h^{\ell-1}|\delta_h|_{2,h}.
\end{aligned}
$$

For the second term we first consider the case $\ell = 2, 3$ and, in view of (H3), introduce, for each edge $e \subset \partial K$, the linear Lagrange interpolant $I^1_{T^{(e)}}$ of δ_h on the triangle $T^{(e)}$, which is obtained by connecting the point x_B (interior to K) and the endpoints of e. Clearly, due to the H^2 regularity of δ_h, the interpolant $I^1_{T^{(e)}} \delta_h$ can be built based on employing the values of δ_h at the vertices of $T^{(e)}$. In particular, using the fact that δ_h is continuous at the endpoints of e we have $[I^1_{T^{(e)}} \delta_h]_{|e} = 0$. Hence, for $\ell = 2$ employing standard interpolation error estimates and a trace inequality we get

$$II \;=\; \sum_e \int_e \partial_n(\Delta u)([\delta_h] - [I^1_{T^{(e)}}\delta_h])ds$$

(23)
$$\lesssim \; h^{2-\frac{1}{2}}|\delta_h|_{2,h}.$$

On the other hand, for $\ell = 3$, we have

$$II \;=\; \sum_e \int_e (I - \Pi^0_e)(\partial_n(\Delta u))([\delta_h] - [I^1_{T^{(e)}}\delta_h])ds$$

(24)
$$\lesssim \; h^2|\delta_h|_{2,h},$$

where we employed the definition of the global space $V_{h,3}$ together with standard interpolation error estimates and a trace inequality. In case $\ell \geq 4$ we have

$$II \;=\; \sum_e \int_e (I - \Pi^{\ell-3}_e)(\partial_n(\Delta u))(I - \Pi^1_e)[\delta_h]ds$$

(25)
$$\lesssim \; h^{\ell-3+1-\frac{1}{2}}h^{1+1-\frac{1}{2}}|\delta_h|_{2,h} = h^{\ell-1}|\delta_h|_{2,h}.$$

Finally, we consider the third term. Using the fact that δ_h is continuous at the vertexes of $\mathcal{T}_h$ and the fact that $\int_e [\delta_h]p\,ds = 0 \; \forall p \in \mathbb{P}^{\ell-3}(e)$ we deduce after integration by parts that $\int_e [\delta_{h,t}]q\,ds = 0 \; \forall q \in \mathbb{P}^{\ell-2}(e)$. Indeed, after observing that for any $p \in \mathbb{P}^{\ell-3}(e)$ there exists $q \in \mathbb{P}^{\ell-2}(e) \setminus \mathbb{P}^0(e)$ such that $p = q'$ we have

$$0 \;=\; \int_e [\delta_h]p\,ds = \int_e [\delta_h]q'ds = -\int_e [\delta_{h,t}]q\,ds + ([\delta_h]q)(\mathsf{v}_2) - ([\delta_h]q)(\mathsf{v}_1)$$
$$=\; -\int_e [\delta_{h,t}]q,$$

where we used the fact that the jump $[\delta_h]$ is zero when evaluated at the endpoints v_1 and v_2 of e. Finally, for $q \in \mathbb{P}^0(e)$ we immediately have, after integration by parts,

$$\int_e [\delta_{h,t}]q = 0.$$

In view of the above result we get

$$III \;=\; \sum_e \int_e (1-\nu)(I - \Pi^{\ell-2}_e)u_{,nt}(I - \Pi^0_e)[\delta_{h,t}]ds$$
$$\lesssim \; h^{\ell-2+1-\frac{1}{2}}h^{\frac{1}{2}}|\delta_h|_{2,h} = h^{\ell-1}|\delta_h|_{2,h},$$

and this concludes the proof. □

5. NUMERICAL RESULTS

The numerical experiments presented in this section are aimed to confirm the a priori analysis developed in the previous sections. To study the accuracy of our new nonconforming method we solve the biharmonic problem (1a)-(1c) on the domain $\Omega =]0,1[\times]0,1[$. The forcing term f in (1a) is set in accordance with the exact solution:

$$u(x,y) = x^2(1-x)^2\,y^2(1-y)^2,$$

which obviously satisfies the boundary conditions in (1b)-(1c).

The performance of the VEM is investigated by observing experimentally the convergence behavior on four different sequences of unstructured meshes labelled by $\{\mathcal{T}_h^{(1)}\}_h$, $\{\mathcal{T}_h^{(2)}\}_h$, $\{\mathcal{T}_h^{(3)}\}_h$, and $\{\mathcal{T}_h^{(4)}\}_h$. All mesh data are reported in Tables 1-4 in the Appendix. Figs. 2(a)-(d) show the first and second mesh of each sequence (top and right plots, respectively). The meshes in $\{\mathcal{T}_h^{(1)}\}_h$, also known as *criss-cross meshes*, are composed by first partitioning Ω in regular square grids and then splitting each square cell into four triangular subcells by connecting the four vertices along the diagonal. It is worth recalling that our nonconforming VEM for $\ell = 2$ on triangular meshes coincides with the Morley finite element method [35]. The meshes in $\{\mathcal{T}_h^{(2)}\}_h$ are built as follows. First, we determine a primal mesh by remapping the position $(\hat{x}, \hat{y})$ of the nodes of a uniform square partition of Ω by the smooth coordinate transformation (see [22]):

$$x = \hat{x} + 0.1\,\sin(2\pi\hat{x})\sin(2\pi\hat{y}),$$
$$y = \hat{y} + 0.1\,\sin(2\pi\hat{x})\sin(2\pi\hat{y}).$$

Then, the corresponding mesh of $\{\mathcal{T}_h^{(2)}\}_h$ is built from the primal mesh by splitting each quadrilateral cell into two triangles and connecting the barycenters of adjacent triangular cells by a straight segment. The mesh construction is completed at the boundary by connecting the barycenters of the triangular cells close to the boundary to the midpoints of the boundary edges and these latter ones to the boundary vertices of the primal mesh. The meshes in $\{\mathcal{T}_h^{(3)}\}_h$ are obtained by filling the unit square with a suitably scaled non-convex octagonal cell, which is cut at the domain boundaries to fit into the unit square domain. The meshes in $\{\mathcal{T}_h^{(4)}\}_h$ are built by partitioning the domain Ω into square cells and relocating each interior node to a random position inside a square box centered at that node. The sides of this square box are aligned with the coordinate axis and their length is equal to 0.8 times the minimum distance between two adjacent nodes of the initial square mesh. All the meshes are parametrized by the number of partitions in each direction. The starting mesh of every sequence is built from a 5×5 regular grid, while for the n-th refined mesh the underlying resolution is $10n \times 10n$. For the virtual element spaces of order $2 \leq \ell \leq 4$ we consider a sequence of 9 meshes; for $\ell = 5$ the calculation is arrested after the fifth mesh when rounding errors begin affecting the accuracy of the approximation due to the

increasing ill-conditioning of the algebraic problem.

For $\ell \geq 2$, we define the relative "$2h$" error by

$$\mathsf{Error}_{2,h} = \frac{|\Pi_\ell^\Delta (u - u_h)|_{2,h}}{|\Pi_\ell^\Delta (u)|_{2,h}}.$$

with $\Pi_\ell^\Delta{}_{|K} = \Pi_\ell^{\Delta,K}$. Thus, on every element $K \in \mathcal{T}_h$, we compare $\Pi_\ell^{\Delta,K} u$, the elliptic projection of the exact solution u and $\Pi_\ell^{\Delta,K} u_h$, the projection of the virtual element solution u_h. These relative errors are shown in the log-log plots of Figs. 3, 4, 5, and 6, with respect to the mesh size parameter h (left panels) and the number of degrees of freedom (right panels). The convergence rate is reflected by the slope of the experimental error curves that are obtained by joining the error values measured on the sequence of refined meshes for each polynomial degree $2 \leq \ell \leq 5$. Each experimental slope has to be compared with the theoretical slope, which is shown for each curve by a triangle and whose value is indicated by the nearby number. From the a priori analysis of Section 4, cf. Theorem 2 and inequality (22)), the $2h$-approximation errors must decrease proportionally to $h^{\ell-1}$ when we use the virtual element space V_ℓ^h. These errors are also expected to decrease proportionally to $|V_h^\ell|^{-\frac{\ell-1}{2}}$, where $|V_h^\ell|$ is the total number of degrees of freedom of the ℓ-th virtual element space, because $|V_h^\ell|$ is roughly proportional to $h^{-1/2}$, Accordingly, the experimental slopes for $\mathsf{Error}_{2,h}$ are expected to be closed to $\ell - 1$ and $(\ell - 1)/2$ when we plot the error curves versus the mesh size parameter h and the number of degrees of freedom. The experimental convergence rates are in perfect agreement with the theoretical ones for all such calculations.

Finally, it is worth mentioning that in a preliminary stage of this work, the consistency of the nonconforming VEM of order ℓ for $2 \leq \ell \leq 5$, i.e., the exactness of the method for polynomial solutions of degree up to ℓ, has been tested numerically by solving the biharmonic equation (1a) with Dirichlet boundary conditions and forcing term determined by the monomials $x^\mu y^\nu$ for all possible combinations of integers μ and ν such that $\mu + \nu \leq \ell$. Non-homogeneous Dirichlet conditions were imposed in strong form by setting the boundary degrees of freedom to the values determined by the exact solution. For these experiments, we considered a wider set of polygonal meshes (including the four considered in this section). In all the cases, the magnitude of the $2h$ errors was comparable to the arithmetic precision, thus confirming the polynomial consistency of the method. We also verified that our nonconforming VEM for $\ell = 2$ on the criss-cross triangular meshes provides the same results of an independent implementation of the Morley finite element method. For the sake of brevity, these results are not reported here.

6. CONCLUSIONS

In this paper we presented the arbitrary-order accurate fully nonconforming virtual element method for biharmonic problems on polygonal meshes. The virtual element space is made of functions that may be globally *not*-continuous. An optimal error estimate in
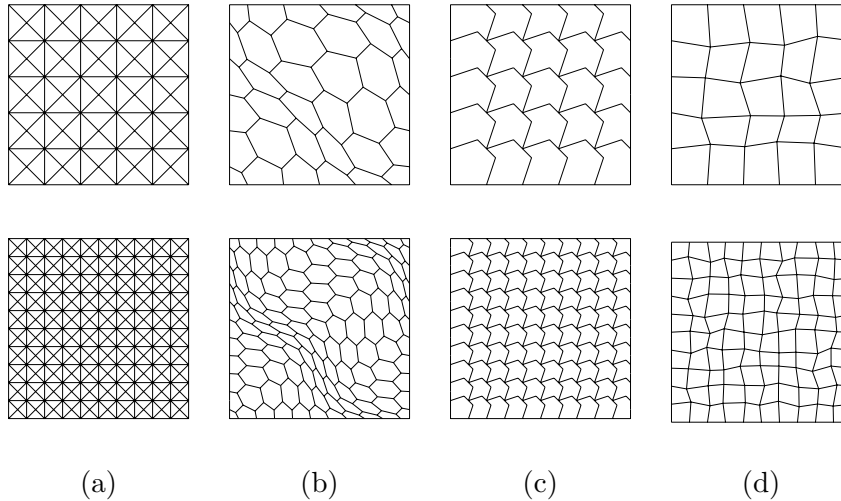
FIGURE 2. Base mesh (top row) and first refinement (bottom row) of the four mesh families: (a) criss-cross triangular mesh; (b) mainly hexagonal mesh; (c) non-convex regular mesh; (d) randomized quadrilateral mesh.

the broken energy norm is derived for all polynomial approximation orders and numerical results assess the validity of the theoretical estimate.

REFERENCES

[1] B. Ahmad, A. Alsaedi, F. Brezzi, L. D. Marini, and A. Russo. Equivalent projectors for virtual element methods. *Comput. Math. Appl.*, 66(3):376–391, 2013.

[2] P. F. Antonietti, L. Beirão da Veiga, D. Mora, and M. Verani. A stream virtual element formulation of the Stokes problem on polygonal meshes. *SIAM J. Numer. Anal.*, 52(1):386–404, 2014.

[3] P. F. Antonietti, L. Beirão da Veiga, S. Scacchi, and M. Verani. A C^1 virtual element method for the Cahn-Hilliard equation with polygonal meshes. *SIAM J. Numer. Anal.*, 54(1):34–56, 2016.

[4] B. Ayuso de Dios, K. Lipnikov, and G. Manzini. The nonconforming virtual element method. *ESAIM Math. Model. Numer. Anal.*, 50(3):879–904, 2016.

[5] L. Beirão da Veiga, F. Brezzi, A. Cangiani, G. Manzini, L. D. Marini, and A. Russo. Basic principles of virtual element methods. *Math. Models Methods Appl. Sci.*, 23(1):199–214, 2013.

[6] L. Beirão da Veiga, F. Brezzi, and L. D. Marini. Virtual elements for linear elasticity problems. *SIAM J. Numer. Anal.*, 51(2):794–812, 2013.

[7] L. Beirão da Veiga, F. Brezzi, L. D. Marini, and A. Russo. $H(\mathrm{div})$ and $H(\mathbf{curl})$-conforming virtual element methods. *Numer. Math.*, 133(2):303–332, 2016.

[8] L. Beirão da Veiga, F. Brezzi, L. D. Marini, and A. Russo. Mixed virtual element methods for general second order elliptic problems on polygonal meshes. *ESAIM Math. Model. Numer. Anal.*, 50(3):727–747, 2016.

[9] L. Beirão da Veiga, F. Brezzi, L. D. Marini, and A. Russo. Virtual element method for general second-order elliptic problems on polygonal meshes. *Math. Models Methods Appl. Sci.*, 26(4):729–750, 2016.

[10] L. Beirão da Veiga, F. Brezzi, L.D. Marini, and A. Russo. Serendipity nodal vem spaces. *Computers and Fluids*, 2016.

[11] L. Beirão da Veiga, A. Chernov, L. Mascotto, and A. Russo. Basic principles of *hp* virtual elements on quasiuniform meshes. *Math. Models Methods Appl. Sci.*, 26(8):1567–1598, 2016.

[12] L. Beirão da Veiga and A. Ern. Preface [Special issue—Polyhedral discretization for PDE]. *ESAIM Math. Model. Numer. Anal.*, 50(3):633–634, 2016.

[13] L. Beirão da Veiga, K. Lipnikov, and G. Manzini. *The mimetic finite difference method for elliptic problems*, volume 11 of *MS&A. Modeling, Simulation and Applications*. Springer, Cham, 2014.

[14] L. Beirão da Veiga, C. Lovadina, and D. Mora. A virtual element method for elastic and inelastic problems on polytope meshes. *Comput. Methods Appl. Mech. Engrg.*, 295:327–346, 2015.

[15] L. Beirao da Veiga, C. Lovadina, and G. Vacca. Divergence free Virtual Elements for the Stokes problem on polygonal meshes. *ArXiv e-prints*, October 2015.

[16] N. Bellomo, F. Brezzi, and G. Manzini. Recent techniques for pde discretizations on polyhedral meshes. *Math. Models Methods Appl. Sci.*, 24:1453–1455, 2014. (special issue).

[17] M. F. Benedetto, S. Berrone, A. Borio, S. Pieraccini, and S. Scialò. Order preserving SUPG stabilization for the virtual element formulation of advection–diffusion problems. *Comput. Methods Appl. Mech. Engrg.*, 311:18–40, 2016.

[18] M. F. Benedetto, S. Berrone, S. Pieraccini, and S. Scialò. The virtual element method for discrete fracture network simulations. *Comput. Methods Appl. Mech. Engrg.*, 280:135–156, 2014.

[19] S. C. Brenner and L. R. Scott. *The mathematical theory of finite element methods*, volume 15 of *Texts in Applied Mathematics*. Springer, New York, third edition, 2008.

[20] S. C. Brenner, K. Wang, and J. Zhao. Poincaré-Friedrichs inequalities for piecewise H^2 functions. *Numer. Funct. Anal. Optim.*, 25(5-6):463–478, 2004.

[21] F. Brezzi, R. S. Falk, and L. Donatella Marini. Basic principles of mixed virtual element methods. *ESAIM: Mathematical Modelling and Numerical Analysis*, 48(4):1227–1240, 2014.

[22] F. Brezzi, K. Lipnikov, and M. Shashkov. Convergence of the mimetic finite difference method for diffusion problems on polyhedral meshes. *SIAM J. Numer. Anal.*, 43(5):1872–1896 (electronic), 2005.

[23] F. Brezzi and L. D. Marini. Virtual element methods for plate bending problems. *Comput. Methods Appl. Mech. Engrg.*, 253:455–462, 2013.

[24] F. Brezzi and L. D. Marini. Virtual element and discontinuous Galerkin methods. In *Recent developments in discontinuous Galerkin finite element methods for partial differential equations*, volume 157 of *IMA Vol. Math. Appl.*, pages 209–221. Springer, Cham, 2014.

[25] A. Cangiani, V. Gyrya, and G. Manzini. The non-conforming virtual element method for the Stokes equations. *SIAM J. Numer. Anal.*, pages 1–25, 2016 (online). DOI:10.1137/15M1049531.

[26] A. Cangiani, G. Manzini, and O. J. Sutton. Conforming and nonconforming virtual element methods for elliptic problems. *IMA J. Numer. Anal.*, pages 1–38, 2016 (online). DOI:10.1093/imanum/drw036.

[27] C. Chinosi and L. D. Marini. Virtual Element Method for fourth order problems: L^2-estimates. *Comput. Math. Appl.*, 72(8):1959–1967, 2016.

[28] P. G. Ciarlet. *The finite element method for elliptic problems*, volume 40 of *Classics in Applied Mathematics*. Society for Industrial and Applied Mathematics (SIAM), Philadelphia, PA, 2002. Reprint of the 1978 original [North-Holland, Amsterdam; MR0520174 (58 #25001)].

[29] A. L. Gain, C. Talischi, and G. H. Paulino. On the virtual element method for three-dimensional linear elasticity problems on arbitrary polyhedral meshes. *Comput. Methods Appl. Mech. Engrg.*, 282:132–160, 2014.

[30] F. Gardini and G. Vacca. Virtual Element Method for Second Order Elliptic Eigenvalue Problems. *ArXiv e-prints*, October 2016.

[31] L. D. Landau and E. M. Lifshitz. *Theory of elasticity*. Course of Theoretical Physics, Vol. 7. Translated by J. B. Sykes and W. H. Reid. Pergamon Press, London-Paris-Frankfurt; Addison-Wesley Publishing Co., Inc., Reading, Mass., 1959.

[32] P. Lascaux and P. Lesaint. Some nonconforming finite elements for the plate bending problem. *Rev. Française Automat. Informat. Recherche Operationnelle Sér. Rouge Anal. Numér.*, 9(R-1):9–53, 1975.

[33] K. Lipnikov, G. Manzini, and M. Shashkov. Mimetic finite difference method. *J. Comput. Phys.*, 257(part B):1163–1227, 2014.

[34] D. Mora, G. Rivera, and R. Rodríguez. A virtual element method for the Steklov eigenvalue problem. *Math. Models Methods Appl. Sci.*, 25(8):1421–1445, 2015.

[35] L. S. D. Morley. The triangular equilibrium element in the solution of plate bending problems. *Aero. Quart.*, 19:149–169, 1968.

[36] I. Perugia, P. Pietra, and A. Russo. A plane wave virtual element method for the Helmholtz problem. *ESAIM Math. Model. Numer. Anal.*, 50(3):783–808, 2016.

[37] G. Vacca and L. Beirão da Veiga. Virtual element methods for parabolic problems on polygonal meshes. *Numer. Methods Partial Differential Equations*, 31(6):2110–2134, 2015.

[38] J. Zhao, S. Chen, and B. Zhang. The nonconforming virtual element method for plate bending problems. *Math. Models Methods Appl. Sci.*, 26(9):1671–1687, 2016.
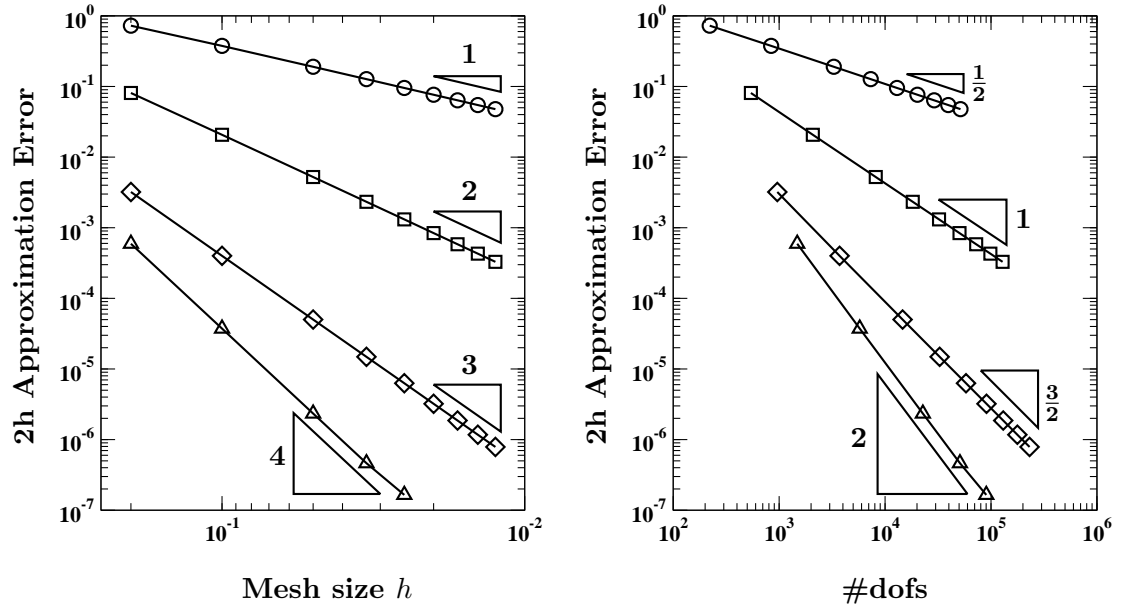
FIGURE 3. Relative $2h$-approximation errors using the sequence of criss-cross triangular meshes versus the mesh size parameter h (left panel) and the total number of degrees of freedom #dofs (right panel).
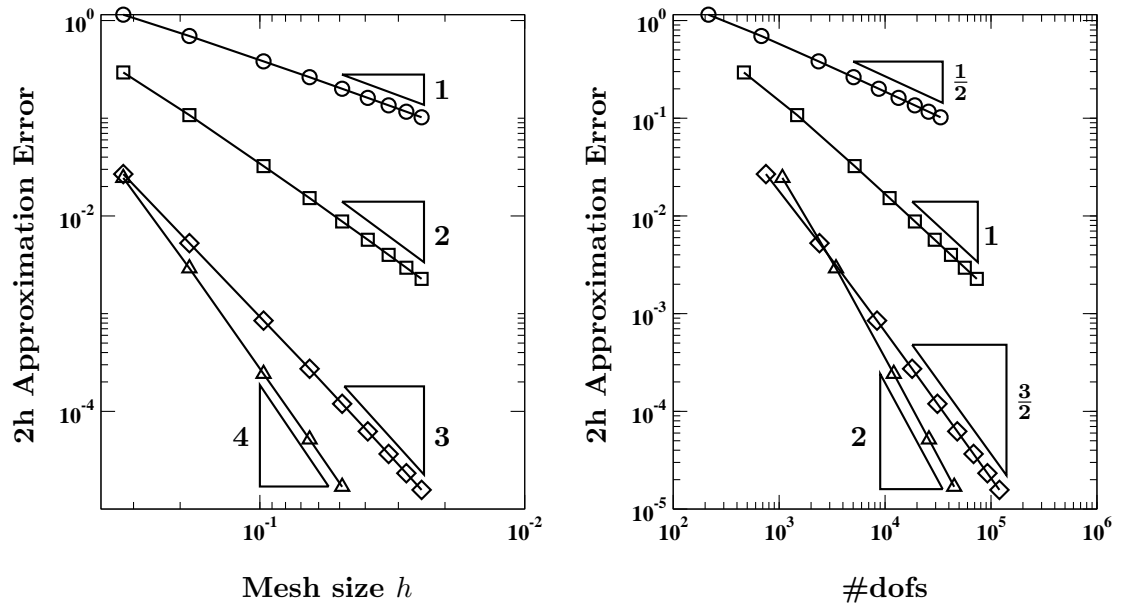

FIGURE 4. Relative $2h$-approximation errors using the sequence of remapped hexagonal meshes versus the mesh size parameter h (left panel) and the total number of degrees of freedom #dofs (right panel).

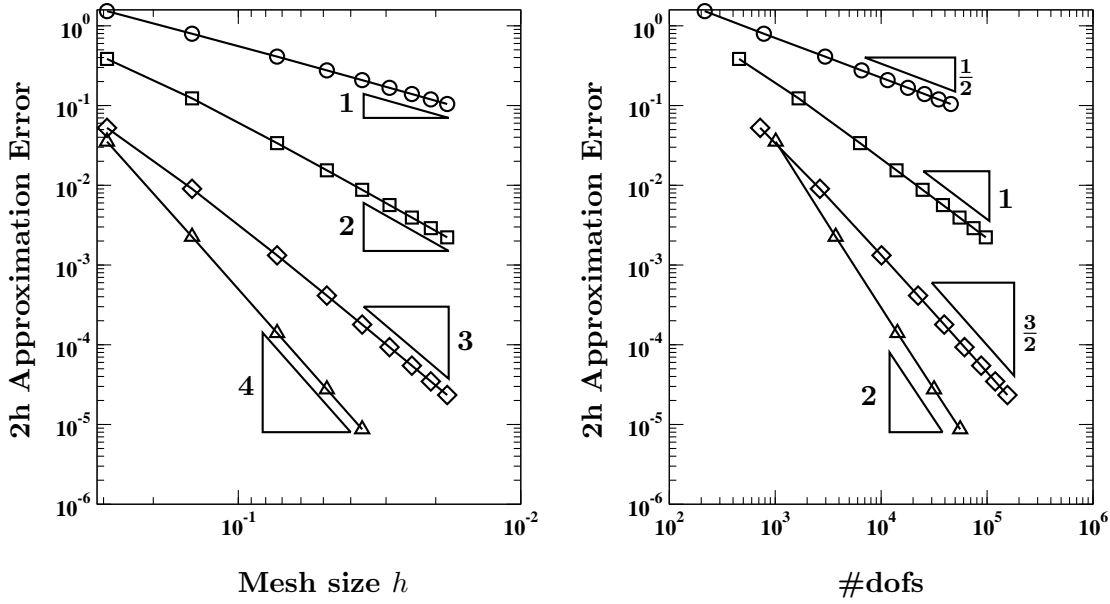FIGURE 5. Relative $2h$-approximation errors using the sequence of non-convex regular meshes versus the mesh size parameter h (left panel) and the total number of degrees of freedom #dofs (right panel).
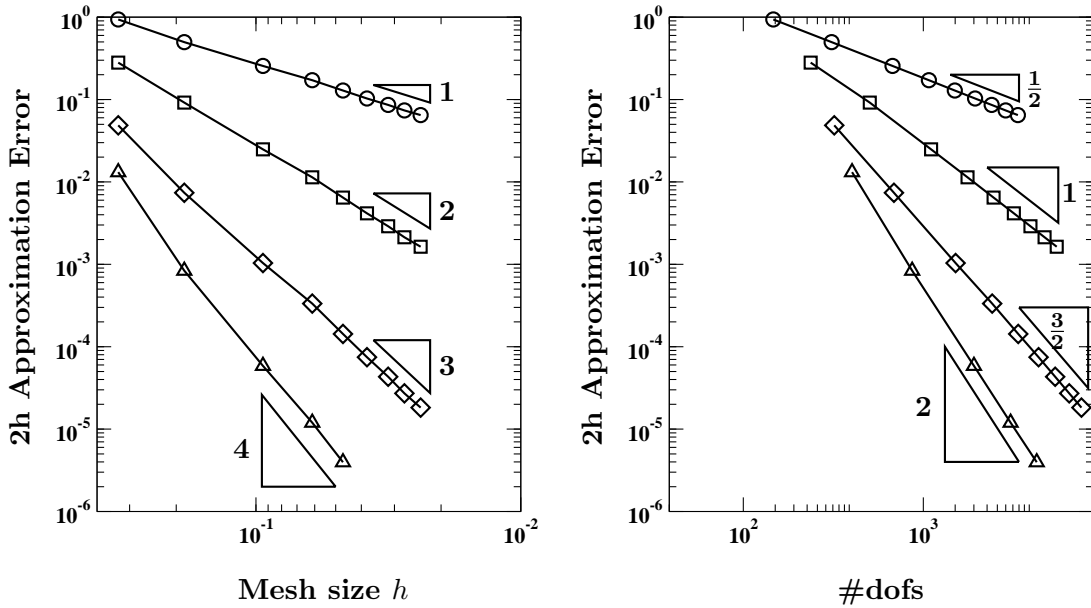
FIGURE 6. Relative $2h$-approximation errors using the sequence of randomized quadrilateral meshes versus the mesh size parameter h (left panel) and the total number of degrees of freedom #dofs (right panel).

APPENDIX

In Tables 1–4, we report the geometric data and the total number of degrees of freedom of the associated VEM spaces for the sequences of considered meshes. More precisely, in Tables 1–4 the first column reports the refinement level $n = 0, 1, 2, \ldots$, the second, third and fourth columns show the corresponding total number of polygonal cells (N_P), faces (N_F) and vertexes (N_V), respectively, whereas in the fifth column the corresponding mesh size h is shown. Finally, in the last four columns we report the total number of degrees of freedom of the corresponding VEM spaces V_h^ℓ, $\ell = 2, \ldots, 5$.

TABLE 1. Geometric data and number of degrees of freedom of the sequence of criss-cross meshes.

n	N_P	N_F	N_V	h	$|V_h^2|$	$|V_h^3|$	$|V_h^4|$	$|V_h^5|$
0	100	160	61	$2.00\,10^{-1}$	221	541	961	1481
1	400	620	221	$1.00\,10^{-1}$	841	2081	3721	5761
2	1600	2440	841	$5.00\,10^{-2}$	3281	8161	14641	22721
3	3600	5460	1861	$3.33\,10^{-2}$	7321	18241	32761	50881
4	6400	9680	3281	$2.50\,10^{-2}$	12961	32321	58081	90241
5	10000	15100	5101	$2.00\,10^{-2}$	20201	50401	90601	$--$
6	14400	21720	7321	$1.67\,10^{-2}$	29041	72481	130321	$--$
7	19600	29540	9941	$1.43\,10^{-2}$	39481	98561	177241	$--$
8	25600	38560	12961	$1.25\,10^{-2}$	51521	128641	231361	$--$

TABLE 2. Geometric data and number of degrees of freedom of the sequence of remapped hexagonal meshes.

n	N_P	N_F	N_V	h	$|V_h^2|$	$|V_h^3|$	$|V_h^4|$	$|V_h^5|$
0	36	125	90	$3.28\,10^{-1}$	215	465	751	1073
1	121	400	280	$1.85\,10^{-1}$	680	1480	2401	3443
2	441	1400	960	$9.69\,10^{-2}$	2360	5160	8401	12083
3	961	3000	2040	$6.49\,10^{-2}$	5040	11040	18001	25923
4	1681	5200	3520	$4.89\,10^{-2}$	8720	19120	31201	44963
5	2601	8000	5400	$3.91\,10^{-2}$	13400	29400	48001	$--$
6	3721	11400	7680	$3.26\,10^{-2}$	19080	41880	68401	$--$
7	5041	15400	10360	$2.80\,10^{-2}$	25760	56560	92401	$--$
8	6561	20000	13440	$2.45\,10^{-2}$	33440	73440	120001	$--$

TABLE 3. Geometric data and number of degrees of freedom of the sequence of nonconvex octagonal meshes.

n	N_P	N_F	N_V	h	$|V_h^2|$	$|V_h^3|$	$|V_h^4|$	$|V_h^5|$
0	25	120	96	$2.91\,10^{-1}$	216	456	721	1011
1	100	440	341	$1.46\,10^{-1}$	781	1661	2641	3721
2	400	1680	1281	$7.29\,10^{-2}$	2961	6321	10081	14241
3	900	3720	2821	$4.86\,10^{-2}$	6541	13981	22321	31561
4	1600	6560	4961	$3.64\,10^{-2}$	11521	24641	39361	55681
5	2500	10200	7701	$2.92\,10^{-2}$	17901	38301	61201	$--$
6	3600	14640	11041	$2.43\,10^{-2}$	25681	54961	87841	$--$
7	4900	19880	14981	$2.08\,10^{-2}$	34861	74621	119281	$--$
8	6400	25920	19521	$1.82\,10^{-2}$	45441	97281	155521	$--$

TABLE 4. Geometric data and number of degrees of freedom of the sequence of randomized quadrilateral meshes.

n	N_P	N_F	N_V	h	$|V_h^2|$	$|V_h^3|$	$|V_h^4|$	$|V_h^5|$
0	25	60	36	$3.311\,10^{-1}$	96	216	361	531
1	100	220	121	$1.865\,10^{-1}$	341	781	1321	1961
2	400	840	441	$9.412\,10^{-2}$	1281	2961	5041	7521
3	900	1860	961	$6.130\,10^{-2}$	2821	6541	11161	16681
4	1600	3280	1681	$4.693\,10^{-2}$	4961	11521	19681	29441
5	2500	5100	2601	$3.808\,10^{-2}$	7701	17901	30601	$--$
6	3600	7320	3721	$3.167\,10^{-2}$	11041	25681	43921	$--$
7	4900	9940	5041	$2.751\,10^{-2}$	14981	34861	59641	$--$
8	6400	12960	6561	$2.389\,10^{-2}$	19521	45441	77761	$--$

P. F. Antonietti: MOX, Dipartimento di Matematica, Politecnico di Milano, Italy
E-mail address: `paola.antonietti@polimi.it`

G. Manzini: T-5 Group, Theoretical Division Los Alamos National Laboratory, New Mexico, USA; Istituto di Matematica Applicata e Tecnologie Informatiche - CNR, Pavia, Italy
E-mail address: `gmanzini@lanl.gov`

M. Verani: MOX, Dipartimento di Matematica, Politecnico di Milano, Italy
E-mail address: `marco.verani@polimi.it`